AGU PUBLICATIONS

JGR

Journal of Geophysical Research: Solid Earth

RESEARCH ARTICLE

10.1002/2013JB010923

Key Points:
- Consistent method for estimating mass balances from GRACE
- Mascon technique
- Evaluate systematic errors GIA correction

Correspondence to:
E. J. O. Schrama,
e.j.o.schrama@tudelft.nl

Citation:
Schrama, E. J. O., B. Wouters, and R. Rietbroek (2014), A mascon approach to assess ice sheet and glacier mass balances and their uncertainties from GRACE data, *J. Geophys. Res. Solid Earth*, *119*, doi:10.1002/2013JB010923.

Received 18 DEC 2013
Accepted 25 JUN 2014
Accepted article online 27 JUN 2014

A mascon approach to assess ice sheet and glacier mass balances and their uncertainties from GRACE data

Ernst J. O. Schrama[1], Bert Wouters[2,3], and Roelof Rietbroek[4]

[1]Faculty of Aerospace Engineering, Delft University of Technology, Delft, Netherlands, [2]Bristol Glaciology Centre, School of Geographical Science, University of Bristol, Bristol, UK, [3]Department of Physics, University of Colorado at Boulder, Boulder, Colorado, USA, [4]Institute of Geodesy and Geoinformation (IGG), Bonn University, Bonn, Germany

Abstract The purpose of this paper is to assess the mass changes of the Greenland Ice Sheet (GrIS), Ice Sheets over Antarctica, and Land glaciers and Ice Caps with a global mascon method that yields monthly mass variations at 10,242 mascons. Input for this method are level 2 data from the Gravity Recovery and Climate Experiment (GRACE) system collected between February 2003 and June 2013 to which a number of corrections are made. With glacial isostatic adjustment (GIA) corrections from an ensemble of models based on different ice histories and rheologic Earth model parameters, we find for Greenland a mass loss of -278 ± 19 Gt/yr. Whereas the mass balances for the GrIS appear to be less sensitive to GIA modeling uncertainties, this is not the case with the mass balance of Antarctica. Ice history models for Antarctica were recently improved, and updated historic ice height data sets and GPS time series have been used to generate new GIA models. We investigated the effect of two new GIA models for Antarctica and found -92 ± 26 Gt/yr which is half of what is obtained with ICE-5G-based GIA models, where the largest GIA model differences occur on East Antarctica. The mass balance of land glaciers and ice caps currently stands at -162 ± 10 Gt/yr. With the help of new GIA models for Antarctica, we assess the mass contribution to the mean sea level at 1.47 ± 0.09 mm/yr or 532 ± 34 Gt/yr which is roughly half of the global sea level rise signal obtained from tide gauges and satellite altimetry.

1. Introduction

Present-day sea level rise has a potentially significant impact on our society because of the economic dependency on the coastal zone. According to *Evelpidou et al.* [2012], local sea level in the Mediterranean changed by 58 ± 5 cm in the last two millennia so that most coastal infrastructure could develop with relatively moderate changes in the mean sea level. Sea level rise since the Roman era is considerably slower than the presently observed 32 ± 4 cm per century estimated from satellite altimetry between 1992 and 2014 [cf. *Church and White*, 2011]. The Intergovernmental Panel on Climate Change projects in its fifth assessment report that sea level is likely to vary between 45 cm and 82 cm relative to the reference period 1985–2005 under the RCP8.5 scenario; see also *Intergovernmental Panel on Climate Change* [2013]. There are several contributions to the sea level rise signal; our working hypothesis is that the associated sea level budget is determined by meltwater fluxes originating from the cryosphere; a second component in the budget is the oceanic volume change as a result of absorption of heat originating from the warming signal into the ocean which affects seawater density. Different observation techniques can be used to identify components that add to the sea level budget. The Gravity Recovery and Climate Experiment (GRACE) satellite mission yields estimates for the mass component; satellite altimetry over the oceans provides the sum of both mass and volume change in the water column. Third, ocean density measurements from conductivity-temperature-depth (CTD), expendable bathythermograph (XBT), and ARGO (website: http://www.argo.ucsd.edu/About_Argo.html last checked 10-jul-2014) profiling floats data are used for ocean volume change, cf. *Leuliette and Willis* [2011] who mention that seawater density changes are observed only in the top 2000 m.

In this paper we focus on the assessment of mass changes for Greenland and Antarctica including Land glaciers and Ice Caps (LIC) with the GRACE system between February 2003 and June 2013, whereby we employ a global mascon modeling strategy. An initial version of the mascon method was used to support the ice mass balance intercomparison study, IMBIE [cf. *Shepherd et al.*, 2012]. Since this project, we have

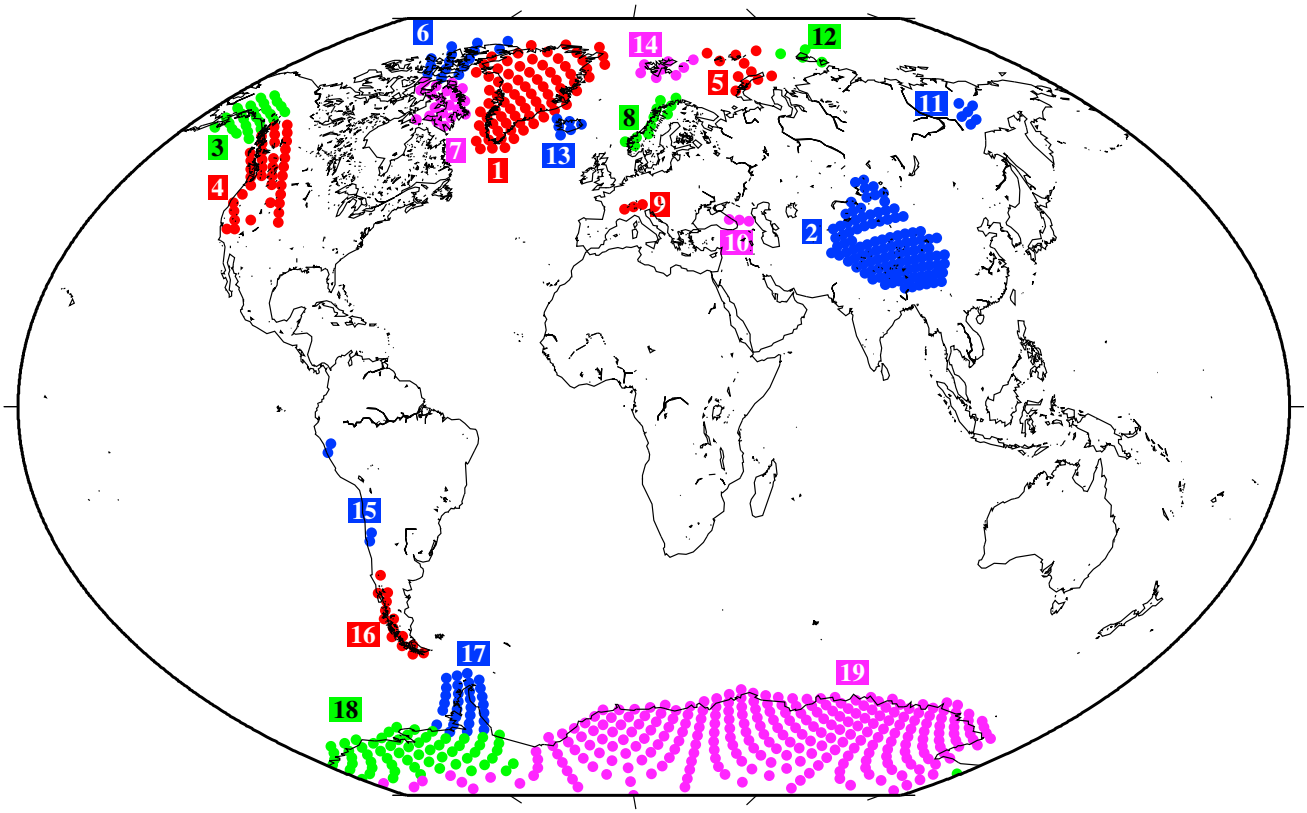

Figure 1. Definition of glaciers and ice caps within the 10,242 mascon set. For the GrIS and the AIS, we allow for an integration area of 200 km around the main ice caps; for land glaciers and ice caps, we follow the definition of the Global Land Ice Measurements from Space (GLIMS) set as discussed in *Raup et al.* [2007] and *Global Land Ice Measurements From Space (GLIMS) and National Snow and Ice Data Center (NSIDC)* [2013]. The areas in this plot are the following: 1: Greenland Ice Sheet, 2: High Mountains Asia, 3: Alaska, 4: Northwest America, 5: Novaya Zemlya and Franz Jozef Land, 6: North Canadian arctic sector, 7: South Canadian arctic sector, 8: Scandinavia, 9: Alps, 10: Caucasus, 11: Siberian glaciers, 12: Severnaya Zemlya, 13: Iceland, 14: Svalbard, 15: North and Middle Andes, 16: Patagonia, 17: Antarctic Peninsula, 18: West Antarctica, and 19: East Antarctica.

increased the number of mascons by a factor of 4, allowing us to derive mass changes for land glaciers and ice caps that were not considered in the IMBIE study. The concept "mascon" stands for "mass concentration" and originates from *Muller and Sjogren* [1968] who have used mascons to model the gravity field of the Moon. Examples of recent approaches that aim at modeling the geopotential regionally use radial basis functions as described in *Eicker et al.* [2014] or use of point-mass modeling techniques [cf. *Baur and Sneeuw*, 2011]. Other examples that rely on mascons are the processing of the GRACE K-band ranging data like cf. *Luthcke et al.* [2013] or use mascons to interpret the regional ice mass loss and glacial isostatic adjustment (GIA) processes as in *Ivins et al.* [2011] or the use mascons to estimate the effect of arctic ocean tides as in *Killett et al.* [2011].

In this paper we define mascons as dishes of approximately the same size that are evenly distributed over the Earth's surface; see also Figure 1. An advantage of the proposed mascon method is that it can be applied to standard GRACE products. A starting point of our analysis is the GRACE level-2 data which consist of monthly geopotential coefficients obtained from the Center of Space Research (CSR) at the University of Austin in Texas to which we add degree 1 and replace degree 2 spherical harmonic coefficients. Differences of monthly geopotential fields relative to their long-term mean are converted into Gaussian smoothed surface water thickness values under the assumption of an elastic Earth model. The obtained surface water thicknesses are in turn converted into mass changes at 10,242 mascons. The time series of the mass changes (mass-time series) at the mascons allow us to reconstruct the mass contribution to the sea level change budget. Hereby, we identify the contributions from the Greenland Ice Sheet (GrIS), Ice Sheets over Antarctica (AIS), and all other remaining Land Glaciers and Ice Caps (LIC). Mass balances for these domains, or components thereof, can only be estimated after correcting for the glacial isostatic adjustment (GIA) effect. We will

use recently published GIA models to assess consequence of GIA model uncertainties in the contribution to the sea level budget. The contribution of the signals from the LIC considers a hydrologic correction to the GRACE data, whereby it is assumed that GRACE observes the sum of LIC sources including a hydrologic signal in watersheds.

We also look into other limitations of the GRACE approach to estimate the mass balances. The GRACE system yields measurements that are affected by the gravitational potential at orbital altitude. In addition, we use a Gaussian averaging function to counteract the natural amplification of errors at high degree and orders in the gravity field. Various tests will be presented to assess the quality of the mass balances estimated from the GRACE data, whereby we will pay attention to GIA model errors. The outline of this paper is as follows: the data processing method starts in section 2 with section 2.1 to highlight the conversion of geopotential into equivalent water thickness, section 2.2 treats the conversion of equivalent water thickness values into mass-time series by mascon, section 3 discusses the mascon inversion algorithm, section 4 shows our results, and the conclusions of our study can be found in section 5.

2. Method

The level-2 GRACE product produced by the CSR consists of monthly spherical harmonic coefficients sets describing the geopotential as seen by the GRACE satellites; see also *Tapley et al.* [2004]. We use the release 5 (RL05) product from the Center of Space Research at the University of Texas at Austin. The coefficient sets $\overline{C}_{lma}(t)$ were obtained from the ftp server at PODAAC (ftp://podaac.jpl.nasa.gov/), where they are stored as so-called GSM files complete to spherical harmonic degree and order 60. An empirical orthogonal function (EOF)-based editing procedure as discussed in *Schrama and Wouters* [2011] is used to identify and remove noisy months that appear as more striped than others in the GRACE data set. This procedure removes all GRACE data in 2002 and several months in 2003 and 2004 so that our final data set contains 119 months between February 2003 and June 2013.

At submonthly time scales, there are various phenomena that result in significant temporal gravity signals that can be seen by the GRACE system. These elastic loading phenomena arise from air pressure variations, ocean and Earth tides, and all other oceanic phenomena that cause mass transport. In the procedure implemented at the CSR, these submonthly effects are removed from the geopotential U; at the same time there are no a priori constraint equations for implementing power laws or smoothness constraints that would affect the parameters in the least squares procedure providing the monthly geopotential coefficient sets; for details, see *Bettadpur* [2007] and *Dobslaw et al.* [2013]. The monthly geopotential parameters should therefore reflect what is only sensed by the GRACE system.

A consequence of the GRACE measurement geometry is that degree 1 geopotential variations are not contained in the monthly coefficient set, and also, the geopotential flattening coefficient $\overline{C}_{2,0}$ becomes less accurate than it is for instance from satellite laser ranging (SLR). For this reason we replace the gravitational flattening coefficient $\overline{C}_{2,0}$ which is poorly observed by GRACE alone, and we add degree 1 coefficients which are associated with geocenter motion that cannot be observed by GRACE alone. Since our goal is to approximate a surface mass layer of the present-day changes, it is also necessary to correct for the glacial isostatic adjustment (GIA) effect which is sensed by GRACE but which should not end up in estimates of the ice sheet mass balances. To determine the contribution of land glaciers and ice caps, we use a land hydrology model to remove hydrologic effects and the details concerning this part will be discussed in section 4.5.

2.1. Conversion of Potential to Water Thickness

For each monthly coefficient set provided at epoch t by GRACE, we define the spherical harmonic coefficients $\Delta\overline{C}_{lma}(t)$ relative to an average from all sets. The $\Delta\overline{C}_{lma}(t)$ coefficients allow one to reconstruct an idealized layer of mass on the Earth's surface which in turn is written as an equivalent water thickness function h so that

$$h(\theta,\lambda;t)=\sum_{l=1}^{L}\sum_{m=0}^{l}\sum_{a=0}^{1}\overline{H}_{lma}(t)\overline{Y}_{lma}(\theta,\lambda) \tag{1}$$

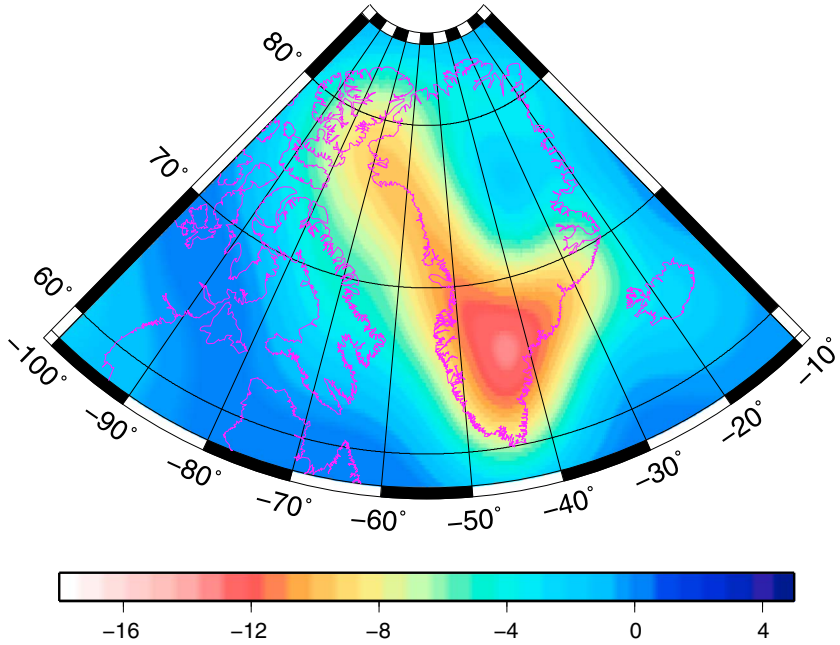

Figure 2. Greenland equivalent water thickness rates expressed in cm/yr computed with a 3° Gaussian smoothing operator; for this map, the GIA effect is modeled with ICE-5G as described in *Paulson et al.* [2007].

where the $\overline{Y}_{lma}(\theta, \lambda)$ functions are associated with normalized spherical harmonics of degree l and order m for co-latitude θ (defined as $\pi/2 - \phi$ where ϕ is the latitude) and longitude λ [cf. *Wahr et al.*, 1998]. The overline operator indicates that the $\overline{Y}_{lma}(\theta, \lambda)$ functions are fully normalized so that

$$\frac{1}{4\pi}\int_{\theta=0}^{\pi}\int_{\lambda=0}^{2\pi}\overline{Y}^2_{lma}(\theta,\lambda)\sin(\theta)\,\mathrm{d}\lambda\,\mathrm{d}\theta = 1 \tag{2}$$

where

$$\overline{Y}_{lma}(\theta,\lambda) = \overline{P}_{lm}(\cos\theta)\begin{cases}\cos(m\lambda) & : a = 0\\ \sin(m\lambda) & : a = 1\end{cases} \tag{3}$$

If an elastic Earth model is assumed, then $\overline{H}_{lma}(t)$ in (1) follows from $\Delta\overline{C}_{lma}(t)$ (or $\Delta\overline{C}_{lm}(t)$ for $a = 0$ and $\Delta\overline{S}_{lm}(t)$ for $a = 1$) by

$$\overline{H}_{lma}(t) = \frac{a_e\rho_e(2l+1)}{3\rho_w(1+k'_l)}W^G_l(\tau_G)\Delta\overline{C}_{lma}(t) \tag{4}$$

In this equation ρ_e and ρ_w are the mean density of the Earth and the specific density of water, a_e, is the mean equatorial radius. To reduce the effect of gravity errors at high degree and order, we insert $W^G_l(\tau_G)$ in equation (4) which is a Gaussian filter as is described in *Swenson and Wahr* [2002]. Four properties are the following:

1. In order to approximate equivalent water thickness values represented by $h(\theta, \lambda; t)$, we rely on a spatial averaging function which is based on Gaussian smoothing as is described in *Swenson and Wahr* [2002]. The purpose of this function is to dampen the effect of the term $(2l+1)$ which naturally amplifies the noise in $\Delta\overline{C}_{lma}(t)$ at higher degrees in (4). As a result, one must define an averaging parameter τ_G in $W^G_l(\tau_G)$.
2. The procedure relies on a set of elastic loading coefficients k'_l for which we have used load Love numbers as specified in *Farrell* [1972]. The procedure for computing mass changes is not significantly affected by the choice of elastic load Love numbers. We find values for the mass change trends that differ by approximately 0.1% when the load Love numbers of *Han and Wahr* [1995] are used instead of those listed in *Farrell* [1972]. However, one must be careful with the definition of load Love number k'_1. When the potential coefficients are expressed relative to the common center of mass, (4) exhibits a singularity for

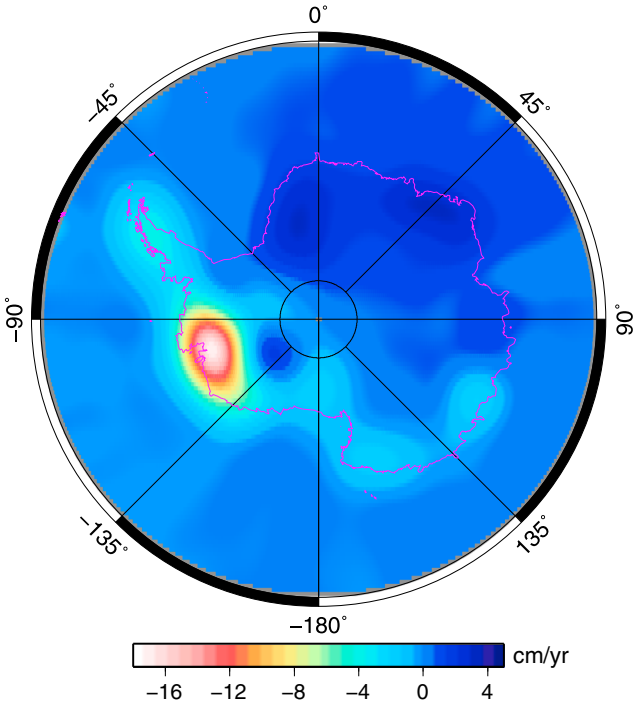

Figure 3. Antarctic equivalent water thickness rates expressed in cm/yr computed with a 3° Gaussian smoothing operator; for this map, we used the best solution of the GIA model described in *Whitehouse et al.* [2012b].

the degree 1 terms. Here we assume $k'_1 = 0.021$ which requires that we augment degree 1 potential coefficients referenced to the center of figure [cf. *Blewitt*, 2003; *Dahlen*, 1976].

3. The series in (1) is truncated at degree L which depends on the GRACE level-2 product and its release number (for the current CSR RL05, $L = 60$).
4. The $\Delta\overline{C}_{lma}$ coefficients are corrected for modeled variations in $h(\theta, \lambda; t)$, i.e., we compensate the glacial isostatic adjustment effect and we replace degree 1 and 2 coefficients as discussed in sections 2.1.1 and 2.1.2.

The rate of change in equivalent water thickness computed with $\tau_G = 3°$ is shown in Figures 2 and 3.

2.1.1. Glacial Isostatic Adjustment Models

Since it is not our intention to retrieve the GIA effect with the GRACE system, we apply a correction based on an a priori model in the conversion as specified in (4). Several GIA models were suggested since the start of the GRACE project or have been proposed at a later point in time as alternatives. Many publications rely on the GIA model of *Paulson et al.* [2007] so that for non-GIA experts, the suggestion may have been raised that the GIA effect was adequately taken out of the GRACE data for ice mass balance studies. We will review this assumption with two alternative ice histories that have resulted in regional GIA models for Antarctica and also alternative ice histories that have resulted in local GIA models for Greenland. When discussing the applied GIA corrections on mass-time series retrieved from GRACE, we refer to the following acronyms:

1. *ICE-5G*. Available are two realizations based on the method described by *Paulson et al.* [2007] who determined an optimum in the viscosity space of the upper and lower mantles with the ICE-5G ice history model and VM2 Earth model from *Peltier* [2004]. One version of the GIA model is based on a compressible Earth model, and an alternative is the incompressible Earth model. In both cases the ICE-5G ice history was assumed; for details, see *A et al.* [2013].
2. *W12a*. In *Whitehouse et al.* [2012b] Antarctica-only GIA models are derived from an updated ice history model discussed in *Whitehouse et al.* [2012a]. We used three realizations, each with different assumptions for the viscosities of the upper and lower mantles, namely, with ν_{um} varying from $8\,10^{20}$ to $1\,10^{21}$ Pa s and ν_{lm} varying from $5\,10^{21}$ to $2\,10^{22}$ Pa s while the lithospheric depth D is either 96 or 120 km.
3. *IJ05_R2*. A new ice history model and corresponding Antarctica-only GIA model is developed by *Ivins et al.* [2013]. In total there are six realizations in the viscosity space for the lower and upper mantles for a lithospheric thicknesses of 65 and 115 km with ν_{um} varying from $2\,10^{20}$ to $4\,10^{20}$ Pa s and ν_{lm} from $1.5\,10^{21}$ to $3.2\,10^{21}$ Pa s.
4. *Simpson*. For the Greenland ice sheet (GrIS), we use eight solutions provided by Glenn Milne within the scope of the IMBIE project, each based on the ice history of *Simpson et al.* [2009]. In total there are eight realizations in the viscosity space, where ν_{um} varies from $3\,10^{20}$ to $1\,10^{21}$ Pa s and ν_{lm} from $1\,10^{21}$ to $1\,10^{22}$ Pa s and a lithospheric thickness D of either 96 or 120 km.
5. *KL/ANU*. In total 27 GIA model realizations are provided by Valentina Barletta within the scope of the IMBIE project who used the TSec computer code. A benchmark study where results from different

computer codes are compared is described in *Spada et al.* [2011], and different solutions for the sea level equation were compared within the EU COST action program ES0701 as described on http://www.cost.eu/. All realizations with the KL/ANU models are based upon an ice history published by *Fleming and Lambeck* [2004]; different viscosities for the upper and lower mantles are assumed, ν_{um} varies from $2\,10^{20}$ to $5\,10^{20}$ Pa s, and ν_{lm} varies from $5\,10^{21}$ to $2\,10^{22}$Pa s, while the lithospheric thickness D varies from 50 to 100 km. The KL/ANU GIA models were provided by Kurt Lambeck at the Australian National University (ANU); the GIA corrections were only applied for calculating mass changes of the Greenland Ice Sheet.

Each of the above described GIA models results in a separate time series for a selected number of mascons which allows us to characterize the GIA model error in the estimated mass balances. In this paper GIA model errors follow from the spread between all time series that form an ensemble for a case to study; this aspect will be discussed in section 4.

2.1.2. Degree 1 and 2 Spherical Harmonics

GRACE cannot directly observe degree $l = 1$ mass loading effects associated with geocenter motions since the equations of motion are formulated in a coordinate system with its origin in the Earth's center of mass. Yet this does not mean that degree $l = 1$ loading effects do not exist, or, that degree $l = 1$ loading effects could not be inferred by combining different geodetic observations types. The existence of degree $l = 1$ loading effects was suggested by *Dahlen* [1976] and demonstrated by *Blewitt et al.* [2001] who analyzed motions of the Earth's crust seen by GPS receivers relative to the GPS space segment. In order to represent mass variations relative to the center of figure of the Earth, rather than the center of mass of the Earth, one needs to add degree $l = 1$ loading coefficients to the GRACE monthly coefficient sets [cf. *Swenson et al.*, 2008]. In our case degree 1 terms follow from replacing the oceanic domain by solutions of the sea level equation, whereby we consider a rotational feedback mechanism as is explained in *Wouters* [2010] with a centrifugal potential that follows from the degree 2 order 1 terms and excitation functions as described in *Sabadini and Vermeersen* [2004]. Our approach is similar to *Swenson et al.* [2008]; in section 4 we describe a comparison and we look at the consequences of considering geocenter corrections for mass balances estimated with GRACE.

The GRACE system is in principle capable of observing the gravitational flattening term $\overline{C}_{2,0}(t)$. However, as was mentioned earlier in this paper, the quality of this information is considered to be worse than obtained from satellite laser ranging (SLR). In earlier publications, such as *Schrama et al.* [2007] and *Schrama and Wouters* [2011], we decided to ignore the degree 2 order 0 geopotential coefficient, and also, we did not include the earlier mentioned degree 1 terms associated with geocenter motions. Within the IMBIE study of *Shepherd et al.* [2012], all GRACE analysis teams agreed to include the degree 1 and 2 contributions. The suggestion to substitute $\overline{C}_{2,0}(t)$ by values obtained from SLR comes from *Cheng et al.* [2013]; a sensitivity study concerning the degree 1 and 2 corrections will be discussed in section 4.

2.2. Mapping of Water Thickness Into Mascons

The forward model discussed in *Wouters et al.* [2008] divides the Greenland Ice Sheet (GrIS) into 16 stream areas including a selected number of adjacent basins such as Ellesmere island, Baffin island, Iceland, and Svalbard. The forward model assumes that each basin is adjusted, whereby it is filled to a (virtual) water level. The procedure is repeated until sufficient coherence is found with the GRACE water thickness values. In *Schrama and Wouters* [2011] the method was rewritten as an inversion procedure, whereby the basin influence functions are multiplied by scaling parameters that are determined by minimizing a quadratic cost function. In both cases the inversion methods assume a local set of basins without considering a significant influence from exterior basins. In *Schrama and Wouters* [2011] we mention that irregularly shaped basins affect the numerical properties of the inversion procedure. In this paper we modify the inversion approach and implement the mascon method on the global domain. Mascons are now defined as a global set of evenly distributed dishes, the generation algorithm in described in Appendix A. All mascons come with a unique response function; the numerical properties of the inversion algorithm are explained in section 3.

We assume that ice sheets and glaciers, for which the mass balances are to be estimated, may be approximated by summing up the mass-time series by mascon retrieved from the inversion algorithm. (For the definition of the integration domains of Greenland and Antarctica, we extended the integration area

250 km into the oceans.) At recursion level 5, for a discussion, see Appendix A, we are able to identify not only the GrIS and the Antarctic Ice Sheet (AIS) but also subdomains such as the Antarctic Peninsula Ice Sheet (APIS), the West Antarctic Ice Sheet (WAIS), and the East Antarctic Ice Sheet (EAIS). At recursion level 6 the mascons become sufficiently dense to also identify Land Glaciers and Ice Caps (LICs). Definitions of the WAIS, the EAIS, and the APIS are taken from *Zwally et al.* [2012] while the definitions of the land glaciers and ice caps are taken from the study of *Jacob et al.* [2012] and *Global Land Ice Measurements From Space (GLIMS) and National Snow and Ice Data Center (NSIDC)* [2013]. Figure 1 shows the color-coded areas that we have identified within the set of 10,242 mascons.

3. Mascon Inversion Algorithm

The purpose of the mascon inversion algorithm is to approximate scaling parameters $\alpha_k(t)$ that appear in the observation equation:

$$h(\theta, \lambda; t) = \sum_{k=1}^{K} \alpha_k(t)\beta_k(\psi_k, L, R) + \epsilon(\theta, \lambda; t) \tag{5}$$

where $\beta_k(\psi_k, L, R)$ are mascon influence functions that follow from a spherical dish truncated at degree L, h is the equivalent water thickness observation derived from (1), $\alpha_k(t)$ denote scaling factors that will be estimated for all mascons at epoch t, and $\epsilon(\theta, \lambda; t)$ is a misclosure term in the observation equation. The term ψ_k is a spherical distance between h on the left-hand side of equation (5) and the kth mascon center. With these definitions the mascon influence function become

$$\beta_k(\psi_k, L, R) = \sum_{l=0}^{L} \gamma_l(R)\overline{P}_l(\cos\psi_k) \tag{6}$$

where R is the radius of a mason and where

$$\gamma_l(R) = \frac{1}{2}\int_{\mu=0}^{R} \overline{P}_l(\cos\mu)\sin\mu\,\mathrm{d}\mu \tag{7}$$

denote the coefficients in a Legendre function expansion of a mascon. In principle the $\gamma_l(R)$ coefficients can be derived from recursive relations for integrals of associated Legendre functions; see *Paul* [1978] which would ensure stability to high degree. However, we only need the coefficients up to $L = 60$ so that γ_l is evaluated with a Gauss-Legendre quadrature summation [cf. *Press et al.*, 1989] and where stable recursive schemes for normatized Legendre functions are used in equation (7). The series expansion in (6) is truncated at degree L as is used in the computation of the equivalent water thickness values h in (4). In Appendix B we describe the possibility of an additional convolution term in equation (6) to study the sensitivity of the mascon inversion algorithm with respect to a spatial averaging.

Now that the observation equations are defined, we implement the inversion algorithm to approximate $\alpha_k(t)$. Input to the algorithm are equivalent water heights collected in vector $\overline{h}$ at the mascon centers; output are approximated scaling factors collected in the vector $\hat{\alpha}$. For the least squares inversion, we evaluate (5) as a system of $2K$ by K equations where the upper part consists of the mascon influence functions contained in A that follow from (6) while the lower part is a unit matrix that implements weak constraint equations required to stabilize the solution. Both parts are multiplied by $P_{\mathrm{h}}^{-1/2}$ and $P_{\mathrm{c}}^{-1/2}$, where P_{h} is the covariance matrix of the observations and P_{c} a covariance matrix for the constraint equations. We assume a scaled unit observation covariance matrix P_{h} and a scaled unit covariance matrix P_{c} to enforce weak constraints on the vector with mascon scaling factors $\overline{\alpha}$. By means of ridge-regression technique, we determine a suitable scale factor between P_{c} and P_{h}; for a discussion, see *Baur and Sneeuw* [2011]. Our conclusion is that $||P_{\mathrm{c}}|| = 10^6||P_{\mathrm{h}}||$ yields a condition where the optimum solution is least affected by the imposed constraints. The constraint equations apply directly to the vector of scaling factors $\overline{\alpha}$ and are taken with a variance that is 10^6 times the observation variance. The result is

$$\begin{bmatrix} P_{\mathrm{h}}^{-\frac{1}{2}}\overline{h} \\ 0 \end{bmatrix} = \begin{bmatrix} P_{\mathrm{h}}^{-\frac{1}{2}}A \\ P_{\mathrm{c}}^{-\frac{1}{2}} \end{bmatrix}\overline{\alpha} + \overline{\epsilon} \;\Rightarrow\; \overline{h}' = A'\overline{\alpha} + \overline{\epsilon} \tag{8}$$

where $\overline{h}$ is a observation vector with equivalent water heights evaluated at the mascon centers, A is an information matrix containing the mascon influence functions from equation (5), A' is a resulting matrix that will

Table 1. Effect of Adding Degree 1 and Replacing Degree 2 Corrections in the Time Frame February 2003 to June 2013[a]

Domain	Rate	$l = 1$	$l = 2$	δ
ANT	-254 ± 21	No	No	
ANT	-208 ± 9	No	Yes	+46
ANT	-221 ± 22	Yes	No	+33
ANT	-176 ± 10	Yes	Yes	+78
GrIS	-274 ± 6	No	No	
GrIS	-265 ± 4	No	Yes	+9
GrIS	-282 ± 6	Yes	No	−8
GrIS	-272 ± 4	Yes	Yes	+2

[a]Column 2 shows the estimated rate in Gt/yr including a two sigma confidence interval, column $l = 1$ shows whether we apply the geocenter correction, and column $l = 2$ shows whether we replaced $\overline{C}_{2,0}$ with SLR observed values. In column δ we show the effect on the mass balances of Greenland and Antarctica. The incompressible ICE-5G GIA correction was used in the calculations.

be subjected to a **QR** decomposition algorithm, vector $\overline{h}'$ is the observation vector augmented with the constraint conditions, and $\overline{\epsilon}$ is a misclore that is minimized by the least squares method.

A least squares approximation is obtained with a **QR** decomposition for which we have used subroutine **DGELS** in the LAPACK library documented in *Anderson et al.* [1990]. The **QR** decomposition algorithm offers the possibility to efficiently solve mass-time series for a set of 10,242 mascons for multiple realizations of $\overline{h}'$ observed by GRACE on the left-hand side of (8). **QR** decomposition is directly applied to a design (or information) matrix A' resulting in an orthonormal matrix Q and an upper triangular matrix R so that any least squares problem like $A^t A\hat{x} = A^t\overline{y}$ can be written as $R\hat{x} = Q^t\overline{y}$.

The centroid-based algorithm described above differs from the grid-based algorithm that we used in, e.g., *Schrama and Wouters* [2011] and that we applied to no more than 20 basins in the GrIS system. Typically, in a grid-based algorithm we estimate parameters $\hat{\alpha}$ from h values provided on a 1°×1° spherical grid:

$$(A^t P_h^{-1} A + P_c^{-1})\hat{\alpha} = A^t P_h^{-1}\overline{h} \tag{9}$$

where $\overline{h}$ contains water thickness values on a grid. With the grid-based algorithm, normal equations and the right-hand side follow from an overdetermined problem where weak constraints stabilize the problem. The efficiency of the grid-based method is a concern since the computational cost is significantly affected by computation of the normal matrix on the left-hand side of (9).

The innovation compared to our earlier research is the use of **QR** decomposition during parameter estimation so that we avoid to compute expensive matrix products like $A^t A$. In addition, mascon influence functions are evaluated at the dish centers rather than a spherical grid. Any matrix product like $A^t A$ is numerically seen less favorable because the resulting spectrum of eigenvalues contains squares of the singular values of the A matrix (singular values are contained in Λ in the singular value decomposition $A = U\Lambda V^t$). A drawback of the **QR** decomposition is an increase in memory allocation compared to the algorithm where $A^t A$ is directly evaluated. The justification for the regularization method used in the **QR** decomposition procedure is that it provides a minimum required stabilization in the estimation procedure; the variance of the constraint equations differs by 6 orders of magnitude compared to the variance assigned to the equivalent water thickness values provided as observations at the mascon centers.

Table 2. Slope (mm/yr), Amplitude (mm), and Phase (as Day Number in the Year) of the Earth's Center of Mass Relative to Its Center of Figure Found by Replacing the Oceanic Domain With a Model Surface That Represents a Gravitational and Rotational Consistent Solution of the Sea Level Equation Driven by Mass Fluxes From Greenland, Antarctica, and the Continents[a]

Computed	Slope	Amplitude	Phase
Δx	-0.06 ± 0.02	1.00	100
Δy	$+0.05 \pm 0.02$	1.38	289
Δz	-0.21 ± 0.03	1.28	81

[a]The computed trend parameters arise from analyzing the present-day effects and depend on the assumed GIA model for the procedure from which we ignored the degree 1 terms.

4. Results

With the centroid-based mascon algorithm discussed in section 3, we retrieve mass-time series at 10242 mascons that describe the mass change for the Greenland Ice Sheet (GrIS) and the Antarctic Ice Sheet (AIS) which consists of three nonoverlapping subdomains: the West Antarctic Ice Sheet (WAIS), the East Antarctic Ice Sheet (EAIS), and the Antarctic Peninsula Ice Sheets (APIS). In addition, we estimate the total mass balance for Land glaciers and Ice Caps (LIC) outside the GrIS and the AIS. During these calculations we correct the gravitational flattening terms and we apply the geocenter loading correction, the

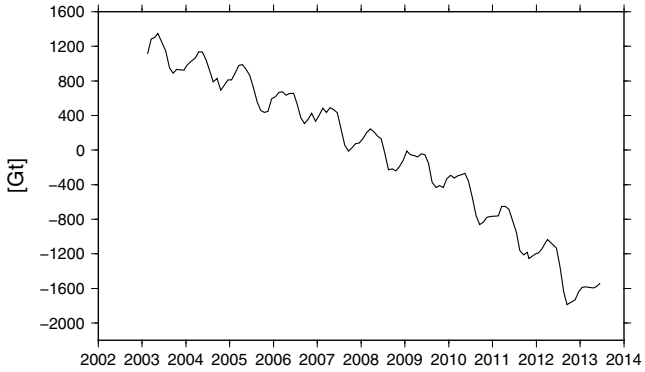

Figure 4. Mass (Gt) of the Greenland Ice Sheet (GrIS) between February 2003 and June 2013 based upon GRACE.

consequences of both corrections are discussed in section 4.1. Sections 4.2 and 4.3 discuss the properties of the mass-time series for the different domains.

4.1. Gravitational Flattening and Geocenter

The mass loss rates for the GrIS and AIS are affected by our choice to add degree 1 geopotential coefficients related to geocenter motions and to replace the $\overline{C}_{2,0}$ coefficients by the results obtained from satellite laser ranging. The consequence of both steps is summarized in Table 1 from which we conclude that replacing the GRACE $\overline{C}_{2,0}$ time series by equivalent SLR data results in mass loss reductions of 46 Gt/yr and 9 Gt/yr for Antarctica and Greenland, respectively. The consequence of modeling degree 1 terms results in a change of the Antarctic and Greenland mass balances by 33 and −8 Gt/yr.

Degree 1 geopotential corrections for analyzing GRACE data were proposed by *Swenson et al.* [2008], *Riva et al.* [2010], and *Rietbroek et al.* [2012b]. In order to estimate the degree 1 terms we assume that the oceanic domain is replaced by a solution of the sea level equation (SLE), where we include a rotational feedback term as explained in *Wouters* [2010] and *Sabadini and Vermeersen* [2004]. Solving the SLE is an iterative process, whereby we determine an ocean correction term; all required convolutions for modeling the required self-attraction and loading potential functions are implemented in the spherical harmonic domain. Input to the algorithm to solve the SLE are the mass changes (from the GrIS, the AIS, the LIC, and the remaining signal on land from GRACE data corrected with the ICE5G GIA model and without application of a hydrology correction). The input consists of the results obtained from the centroid-based mascon inversion method for which we separately calculate water height thickness values that are not corrected by degree 1 terms. In addition, we restore the GAD ocean correction (for details see [*Bettadpur*, 2007]) in the level-2 GSM data set, the $\overline{C}_{2,0}$ parameter is replaced by the time series obtained from SLR data, and the GSM spherical harmonic coefficients are corrected for the GIA effect with the Paulson GIA model.

After replacing the oceanic domain by our model ocean function, we estimate geocenter variations from the relation:

Table 3. Annual Spring to Autumn Mass Loss Observed by GRACE Over the GrIS (Gt)[a]

Year	M_{max}	M_{min}	δ	σ	t_{max} (Spring)	t_{min} (Autumn)
2003	262	−191	453	48	2003.36	2003.71
2004	201	−236	437	51	2004.29	2004.79
2005	261	−286	547	49	2005.29	2005.79
2006	153	−210	363	65	2006.20	2006.71
2007	219	−273	492	40	2007.29	2007.71
2008	237	−243	480	43	2008.21	2008.79
2009	188	−227	415	64	2009.04	2009.71
2010	262	−323	585	34	2010.37	2010.71
2011	315	−279	594	55	2011.29	2011.83
2012	334	−411	745	78	2012.26	2012.70

[a]Columns M_{max} and M_{min} show the deviation relative to the year average of the mass signal, columns t_{max} and t_{min} show the corresponding epochs, δ shows the difference between columns M_{max} and M_{min}, and σ is the estimated standard deviation of δ and estimated from high-pass filtered mass-time data at a cutoff periodicity of 6 months. GRACE sees the largest positive mass deviation in the autumn and the negative in the autumn. Note that the largest spring to autumn mass losses over the GrIS occur since 2010. Since 2013 was not complete, we did not include it in this table.

$$\Delta x_i = \frac{1}{M_e}\int_\Omega \Delta m(\bar{x}) x_i \, d\Omega \quad \forall \; i \in [1,3] \tag{10}$$

where M_e is the Earth's mass and $\Delta m(\bar{x})$ the mass change at location $\bar{x}$. This integral is approximated with the help of the results obtained from the mascon inversion algorithm. Although the procedure followed by *Swenson et al.* [2008] differs compared to ours, we find a correlation better than 0.86 between the geocenter motions reconstructed from both time series. Annual amplitude and phase and drift parameters for the geocenter motion are listed in Table 2, whereby it should be remarked that the drift term found for the *z* axis of the geocenter is of direct concern for the mass balance estimation. Not applying a value of

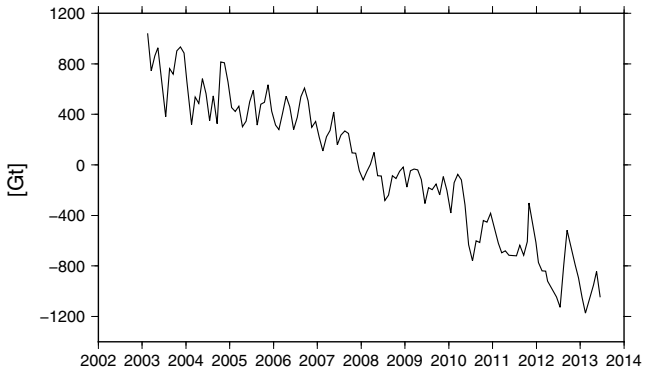

Figure 5. Mass-time series of the Antarctic Ice Sheet corrected with the W12a model (Gt).

−0.21 mm/yr, see Table 2, for the *z* axis of the geocenter results in a significant overestimation of the Antarctic mass balance; see also Table 1, *Ivins et al.* [2013], and *Shepherd et al.* [2012].

An independent geodetic verification of the variations in geocenter motion is in our opinion challenging, since the values found by the procedure here and those in *Swenson et al.* [2008] both tend to show smaller annual amplitudes than from an analysis of GPS station coordinates as reported in, e.g., *Lavallée et al.* [2006]. Space-geodetic values for the geocenter based on GPS and SLR arrive at larger annual amplitudes because atmospheric loading is included in their estimates (J. C. Ries, personal communication, 2014), while we corrected for all ocean and atmospheric effects prior to deriving equivalent water thickness values. In the paper of [*Rietbroek et al.*, 2012a] a number of geodetic techniques are combined to arrive at a present-day degree 1 contribution to the geocenter motion of $\dot{z} = -0.37$ mm/yr.

4.2. Greenland

The mass-time series for the GrIS is shown in Figure 4. The data displayed in this figure are based upon geopotential coefficients corrected for the GIA effect based on the ICE-5G model, degree 1 loading coefficients for modeling variations in the geocenter location, and gravitational flattening coefficients $\overline{C}_{2,0}$ taken from satellite laser ranging (SLR) solutions [cf. *Cheng et al.*, 2013]. The equivalent water thickness fields are computed with a 2.25° Gaussian smoothing and the centroid-based mascon algorithm as discussed in section 3 are applied to derive a minimum constrained solution at 10,242 nodes.

From the data shown in Figure 4, we see that there are yearly maxima in the spring and minima in the autumn superimposed on a longer trend function that is clearly linear and parabolic as was suggested by *Velicogna* [2009]. The rate of mass loss in Figure 4 follows from fitting a trend model to the mass-time series. The outcome of this procedure depends on a number of assumptions, namely, the time window over which a trend function $M(t)$ is computed, and whether (for instance) sine and cosine terms at the annual frequency are incorporated in the trend function. We assume the trend function:

$$M(t) = a_0 + a_1(t - t_0) + \frac{1}{2}a_2(t - t_0)^2 + a_3 \cos\omega(t - t_r) + a_4 \sin\omega(t - t_r) \tag{11}$$

where $t_0 = \frac{1}{2}(t_1 + t_2)$ is an offset time with t_1 and t_2 the extremes of t counted in decimal years and $t_r = 2000$. For each area D in Figure 1 to investigate, we generate a signal that is obtained from the sum of all involved mascon, the accumulated signal results in a time series $M_D(t)$. The parameters a_i in equation (11) are now estimated by fitting the function $M(t)$ to observations $M_D(t)$. This results in estimates for the mass change rate and acceleration a_1 and a_2 that represent averages over the interval $[t_1, t_2]$ while a_3 and a_4 provide information about the annual amplitude and the phase of the signal within area D.

Figure 6. Mass-time series found by GRACE for the West Antarctic Ice Sheet (Gt).

The estimated rate and acceleration terms depend on the choice of t_1 and t_2 and data distribution. In reality we miss only a few GRACE months, i.e., we omit those months where the GRACE

Figure 7. Mass-time series found by GRACE for the ice sheets and glaciers on the Antarctic Peninsula (Gt).

satellites fly in a deeply resonant (repeating) ground configuration so that the CSR solutions become noisy. The reason for this type of noise in the CSR coefficient sets is that the degree and order 60 spherical harmonic development are overparameterizing a potential field that is only mapped along tracks that repeat in a geographical sense, whereas in nonrepeating GRACE configurations the geopotential field is more evenly covered. The "noisy months" identification procedure relies on EOF decomposition of the equivalent water thickness data matrix as is explained in *Schrama and Wouters* [2011].

The trend function parameters a_i in (11) each come with a confidence interval. If one time-mass series is available, then the confidence region follows from the inverse of the normal matrix to determine a_i in (11). In this case the parameter variance depends on the observation variance, where the input signal follows from summing over the mascons that constitute an area D. We use an iterative variance calibration method to assess the monthly observations in $M_D(t)$, so that the variance of the residuals of $\overline{M}_D - \overline{M}$ is in agreement with the observation variance of $M_D(t)$ [cf. *Koch*, 1999]. A diagonal observation variance matrix is assumed because there is no known reason to assume that the GRACE geopotential coefficient sets are correlated from month to month. However, this is not true when geophysical model corrections are applied during the GRACE data processing. The choice of the GIA model is a direct concern, because it provides a trend correction to the mass change. For this reason a different parameter variance assessment method is used when more than one GIA model is available or when other variations are allowed in the processing scheme to define $M_D(t)$. In this case there is an ensemble of time-mass series, and the variance to assign to parameters in the function model $M(t)$ depends on the parameter variance following from the normal matrix to which we add the variance that follows from the distribution of individual parameters of $M(t)$ within the ensemble.

In this way we find for the GrIS that the rate of mass loss becomes -227 ± 10 Gt/yr with an acceleration of -18 ± 5 Gt/yr^2 for calendar years 2003 to 2010. These trend parameters come with a 95% confidence interval equivalent twice the standard deviation of the trend and the acceleration, respectively. For this calculation we assume that (1) the ensemble of the compressible and the incompressible Paulson GIA correction applied to the GRACE gravity data, (2) a Global Land Data Assimilation System (GLDAS) model correction which is required to remove an predicted hydrologic contribution on land, (3) a new $\overline{C}_{2,0}$ coefficient series from SLR data, and (4) a geocenter correction as described in section 4.1. Without exception the estimated mass balance of the GrIS is negative so that the summer loss exceeds the winter gain. To illustrate this effect we show in Table 3 the spring to autumn mass change as seen by GRACE. For 2003 to 2009, both methods show a spring to autumn mass change of approximately 450 ± 100 Gt; for 2010 and onward, we observe that the rate of mass loss of the GrIS increases. With the same method the GrIS mass balance we find -270 ± 9 Gt/yr and -31 ± 3 Gt/yr^2 between February 2003 and June 2013.

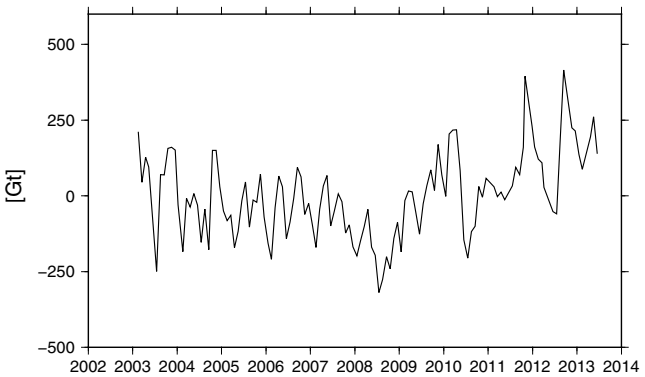

Figure 8. Mass-time series for the East Antarctic ice sheet (Gt).

Our results for the GrIS agree with the values shown in *Velicogna* [2009], *van den Broeke et al.* [2009], *Schrama et al.* [2011], *Shepherd et al.* [2012], and *Wouters et al.* [2013a], where it is shown that the GrIS and Antarctic ice sheet mass losses are accelerating. More difficult is to assess the correction model uncertainties in the GrIS mass balances

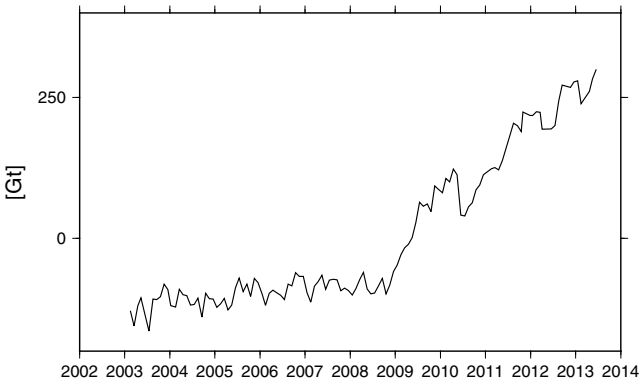

Figure 9. Mass-time series over Dronning Maud land, this series suggests a mass balance of approximately 15 ± 2.5 Gt/yr between February 2003 and May 2009, which is suddenly followed by a mass increase of $\approx$ 300 Gt up to the end of the time series in June 2013. This effect is confirmed by a surface mass balance estimation that is independent of the GRACE observation technique; for details, see *Shepherd et al.* [2012] and *Boening et al.* [2012].

estimates derived from GRACE, and in particular, whether these effects are related to GIA modeling errors and degree 1 and 2 effects. The level at which the GIA model errors occur is evaluated by repeating the same mass balance calculation with different a priori corrections followed by an evaluation of the generated ensemble of solutions. The ensemble method assumes that all used correction methods reflect the present-day knowledge for instance of not only the GIA signal on Greenland but also the used degree 1 and 2 correction methods.

For GIA uncertainties on the GrIS, we consider in analogy to *Shepherd et al.* [2012] 37 models based upon Simpson, ICE-5G, and KL/ANU as explained section 2.1.1. These GIA models reveal different ice histories and Earth model parameters like viscosity for the upper and lower mantles and lithospheric thickness. The trend function is now reevaluated with an ensemble of time series, and we come to the conclusion that the GrIS is changing mass at a rate of -278 ± 19 Gt/yr and an acceleration of -31 ± 3 Gt/yr^2 between February 2003 and June 2013, which is within the confidence region that we got for the GrIS mass balance based on GRACE data corrected with the ICE-5G GIA model ensemble. The Simpson GIA model ensemble results in -267 ± 16 Gt/yr, and the KL/ANU model ensemble results in -281 ± 14 Gt/yr.

4.3. Antarctica

We divided the Antarctic continent into ice sheets on the Peninsula (APIS), West Antarctica (WAIS), and East Antarctica (EAIS); see also Figure 1. The mass-time curve for Antarctica (and all the subdomains discussed in this section) obtained with the W12a GIA model correction applied to the GRACE data is shown in Figure 5. The largest mass losses on Antarctica occur within the Amundsen sea sector (AMUD) and on the Antarctic Peninsula; for reference, see Figure 3. The mass loss on the Antarctic Peninsula between February 2003 and June 2013 is shown in Figure 6; according to this realization, we find -37 ± 4 Gt/yr and -4 ± 1.4 Gt/yr^2. Within the same time frame we get for West Antarctica, see Figure 7, a mass change of -145 ± 6 Gt/yr and -25 ± 3 Gt/yr^2. The mass-time curve for East Antarctica is shown in Figure 8 and the trend is 91 ± 14 Gt/yr and 18 ± 5 Gt/yr^2. The overall characteristics of the time series of all three ice sheets on Antarctica differs compared to what we find on the GrIS. West Antarctica shows a statistically significant acceleration effect, while this is not the case on the Peninsula or East Antarctica. None of the three ice sheets shows a clear annual

Table 4. The Average Rate of Mass Loss Including a 95% Confidence Interval for Subdomains of the AIS Based Upon an Ensemble of the IJ05_R2 and W12a GIA Model Realizations and for the GrIS Based Upon an Ensemble of the Simpson, KL/ANU, and Paulson GIA Model Realizations Between February 2003 and June 2013[a]

Domain	IJ05_R2	W12a	SAI	Acc
AIS	-93 ± 29	-91 ± 23		-12 ± 7
WAIS	-129 ± 9	-145 ± 6		-25 ± 2
EAIS	69 ± 19	91 ± 14		18 ± 5
EAIS*	48 ± 20	70 ± 16		7 ± 16
APIS	-33 ± 3	-37 ± 4		-4 ± 2
AMUD	-107 ± 2	-113 ± 2		-15 ± 1
GRIS			-278 ± 19	-31 ± 3

[a]All values are in Gt/yr or Gt/yr^2. For the AIS and its subdomains, columns "IJ05_R2" and "W12a" show the values obtained by the corresponding GIA models, and column "SAI" shows the Simpson, KL/ANU, and ICE-5G GIA model combination which consists of an ensemble of 37 samples; see section 2.1.1 for a discussion. The mass changes for domain EAIS* refer to February 2003 to June 2009 so that we exclude the extreme mass gain over the Dronning Maud land region that started since June 2009; see Figure 9. The GLIMS data set includes peripherical glaciers on East and Northeast Greenland and peripheral glaciers on the Antarctic peninsula. All peripheral glacier systems in GLIMS are included in the domains of the GrIS and the APIS.

Table 5. Mass Change Rates in Gt/yr and Accelerations in Gt/yr^2 Estimated From Mass-Time Series and Their 95% Confidence Interval Determined by the Residual of the Trend Model and Realizations[a]

Domain	Rate1	Acc1	Rate2	Acc2
GRIS	-270 ± 9	-31 ± 3	-227 ± 10	-18 ± 5
AIS	-171 ± 22	-12 ± 7	-156 ± 24	-14 ± 13
EAIS	19 ± 15	18 ± 5	-1 ± 16	19 ± 10
WAIS	-151 ± 7	-25 ± 3	-119 ± 7	-29 ± 4
AMUD	-107 ± 2	-15 ± 1	-89 ± 2	-17 ± 2
APIS	-40 ± 2	-4 ± 1	-36 ± 3	-4 ± 3

[a]Column "Domain" lists the Greenland Ice Sheet (GrIS) and the West Antarctic Ice sheet (WAIS), where AMUD is for glaciers ending up in the Amundsen section; the AMUD represents a subsection within the WAIS. The East Antarctic Ice Sheet (EAIS) and the Antarctic Peninsula Ice Sheets (APIS) are subdomains of the Antarctic Ice Sheet (AIS). Columns "rate1" and "acc1" show the trends for the time window February 2003 to June 2013, while columns "rate2" and "acc2" are trend parameters for 2003 to 2010. The GIA effect is modeled with the ICE-5G GIA model ensemble.

variation like observed on the GrIS. In Table 5 we summarize rates and accelerations of the GrIS and the AIS including its subdomains.

For the EAIS, one should remark that a strong mass accumulation occurred on Dronning Maud land starting in June 2009 as is shown in Figure 9; see also *Boening et al.* [2012]. For this reason the East Antarctic ice sheet mass change is 70 ± 16 Gt/yr up to June 2009, which is changed to 91 ± 14 Gt/yr for the full time window running from February 2003 to June 2013 when the W12a model ensemble is used.

4.4. The GIA Correction of the AIS

A first assessment of GIA model uncertainties affecting geodetic observation techniques was provided in *James and Ivins* [1995]. In *Wahr et al.* [2000] a solution is proposed to combine satellite altimetry and gravimetry for estimating the Antarctic mass balance to overcome the problems seen with existing GIA models for Antarctica. The conclusion of both studies is that the GIA correction has a significant effect on the Antarctic Ice Sheet mass balance. This finding is confirmed by *Gunter et al.* [2009] who show mass balances for the AIS from GRACE and ICESat with GIA models based on ICE-5G and IJ05, i.e., the previous release of IJ05_R2. Also in *Velicogna* [2009] the GIA signal is addressed for Antarctica; their conclusion is that the correction itself is as large as the rate of mass loss. To demonstrate the sensitivity of the AIS for GIA model errors we calculated the AIS mass balances without the GIA correction so that one finds -3 ± 18 Gt/yr between February 2003 and June 2009 which is statistically seen incompatible with the setup where the ICE-5G model ensemble is used.

Table 6. Rates of Mass Change in Gt/yr Including the 95% Confidence Interval for Land Glaciers and Ice Caps Between February 2003 and June 2013[a]

Domain	GLDAS Corrected	No Correction
Alaska	-35.1 ± 2.8	-35.0 ± 2.8
Alps	-1.0 ± 0.3	-0.2 ± 0.3
Andes	1.5 ± 0.6	-0.3 ± 0.6
Northern Canadian Arctic	-33.9 ± 3.3	-33.7 ± 3.3
Southern Canadian Arctic	-28.4 ± 1.9	-27.9 ± 1.9
Caucasus	0.1 ± 0.4	-0.6 ± 0.5
High Mountains Asia	-16.5 ± 3.8	-16.5 ± 4.4
Iceland	-8.6 ± 0.6	-8.6 ± 0.6
New Zealand	0.3 ± 0.4	0.1 ± 0.3
Nova Zemlya and FJL	-5.8 ± 0.9	-5.7 ± 0.9
North West America	1.7 ± 2.5	3.8 ± 2.7
Patagonia	-13.1 ± 1.6	-13.1 ± 1.5
Scandinavia	0.7 ± 0.9	1.3 ± 0.9
Severnaya Zemlya	-0.9 ± 0.2	-0.8 ± 0.2
Siberia	0.8 ± 0.6	0.8 ± 0.6
Svalbard	-4.3 ± 0.6	-4.0 ± 0.7
LIC	-142.7 ± 7.8	-140.3 ± 8.0

[a]FJL stands for Franz Jozef Land. We have assumed that the Canadian Arctic sector consists of a northern and a southern part separated at 74°N that includes Ellesmere and Baffin Island. The ICE-5G GIA model ensemble was assumed for these calculations; no little ice age correction is considered in this table.

A new element in the discussion is the availability of updated historic ice heights for Antarctica which is a different approach than to modify the Earth model parameters with the same historic ice height model as is pursued in, for instance, *Wahr et al.* [2000]. In this context we consider two new GIA models (W12a and IJ05_R2; for a description, see section 2.1.1) based on new ice history data of Antarctica. For both models, GPS uplift rates constrain the viscosity and lithospheric thickness parameters in the Earth model. We apply an ensemble approach with three solutions based on different Earth model parameters and the W12a ice history and likewise six realizations with the IJ05_R2 model. From all cases, we obtain an ensemble that results in a mean and corresponding 95% confidence region.

The results are shown in Table 4, where we take note that the total Antarctic mass balance is estimated at

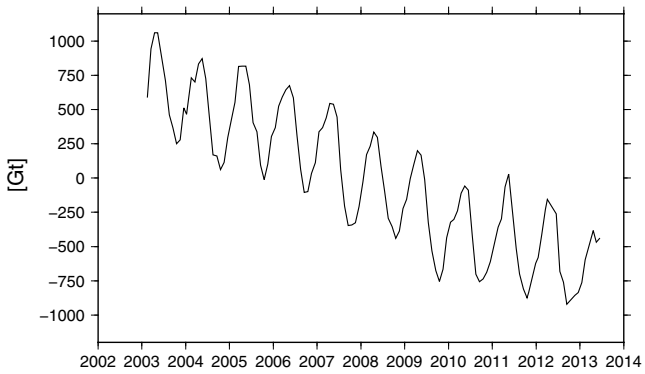

Figure 10. Mass-time series of cumulative effect of land glaciers and ice caps.

−93 ± 29 Gt/yr when six realizations of the IJ05_R2 model are used in an ensemble approach. For the W12a model, we have three realizations; in this case the mass loss for the AIS becomes −91 ± 23 Gt/yr. Both ensemble estimates demonstrate that we reduce the AIS mass balance by approximately 50% as a result of a new ice history rather than a variation in the viscosity of lithospheric thickness parameterization in the calculation of the GIA effect. Another variation in the GIA model calculation is to allow a compressible Earth model, whereas normally incompressible models are assumed; this modification does not significantly alter the AIS mass balance; in fact, it results in a 1% change of the AIS mass balance [cf. *A et al.*, 2013]. Our conclusion is that the values shown in Table 4 differ significantly from the mass rates shown in Table 5 which are derived from the ICE-5G GIA model ensemble.

4.5. Land Glaciers and Ice Caps

Table 6 shows the estimated rates of mass loss for land glaciers and ice caps (LIC); in Figure 10 we show the mass-time series of the total LIC signal. We summarized all land glaciers and ice sheets based on the inventory shown in *Jacob et al.* [2012], whereby we rely on the definitions in the GLIMS data set made available by Bruce Raup from the University of Colorado; see also *Raup et al.* [2007] and *Global Land Ice Measurements From Space (GLIMS) and National Snow and Ice Data Center (NSIDC)* [2013]. Two values are presented in Table 6 for each domain depending on whether a soil moisture effect in the first 2 m and a snow water equivalent layer is removed. These effects are predicted with the GLDAS NOAH model, see *Rodell et al.* [2004], provided by the Goddard Earth Sciences Data and Information Services Center.

The GLDAS model predicts values in kg/m^2 globally with the exception of Antarctica. We exclude GLDAS predictions over Greenland and permafrost regions because of quality considerations and rely on the estimated values of soil water in four layers up to a depth of 2 m and the snow water equivalent information within GLDAS. These data are represented on a 1° × 1° spherical grid at 3-hourly time steps. The monthly mass change is obtained by integrating the GLDAS-predicted water storage within a time window compatible with the used GRACE data.

In this implementation the GLDAS surface water model predictions are conservative in the sense that the model generally predicts less signal than found with GRACE, perhaps because the GLDAS model does not forecast the mass changes associated with the deeper ground water, perhaps because we miss the permafrost changes. More details on this phenomenon are discussed in, e.g., *Jensen et al.* [2013]. In the end the GLDAS model results in a continental hydrology correction to the GRACE data except for land glaciers, ice sheets, and permafrost; see also the studies of *Rodell et al.* [2004] and *Jacob et al.* [2012].

Table 7. Zonal Averages for the Rate of Mass Change on Land in Gt/yr[a]

Band	Gt/yr	N	mm/yr
above 70°N	−0.7 ± 3.5	54	−0.35
50°N to 70°N	2.7 ± 15.2	494	0.14
30°N to 50°N	−45.3 ± 10.6	524	−2.23
10°N to 30°N	−40.0 ± 12.4	545	−1.90
10°S to 10°N	48.2 ± 16.5	393	3.17
30°S to 10°S	84.3 ± 13.7	402	5.41
50°S to 30°S	−26.3 ± 2.7	104	−6.54
70°S to 50°S	0.2 ± 0.3	3	1.60
below 70°S	−3.2 ± 0.9	14	−5.87

[a]N stands for the number of mascons by latitude band and mm/yr represents the average change by latitude band.

The conclusion is that the LIC signal contributes −143 ± 8 Gt/yr to the sea level; see also Table 6. Solid Earth effects associated with the Little Ice Age (LIA) attribute −19 ± 6 Gt/yr to the LIC signal, hereby we refer to the correction mentioned in *Jacob et al.* [2012], so that the LIC signal becomes −162 ± 10 Gt/yr. The LIA correction adds −7 ± 4 Gt/yr to Alaska, −3 ± 1 to the HMA, and −9 ± 5 to Patagonia. With this implementation of the hydrology correction from GLDAS we find small changes in the LIC trend. The LIC signal over Northwest America, area "4" in Figure 1, sees the largest change after

application of the GLDAS correction. But this is not true for all hydrology models considered by *Wouters et al.* [2013b], who determine −21 ± 40 Gt/yr for the total hydrologic correction, i.e., the effect is not statistically different from zero. An uncertainty in the hydrologic correction means that one cannot separate ice from water mass variations on land, yet this does not affect the total contribution to the sea level observed by GRACE.

Hydrologic mass trends on land outside glaciers and ice caps are listed in Table 7. The total contribution of this part of the domain to the global sea level is not statistically significant from zero in the GRACE data since we find 20 ± 33 Gt/yr; however, the analysis shows that there is a zonal preference in the signal where GRACE shows a mass gain at tropical latitudes while the continents become dryer at subtropical and moderate latitudes.

5. Conclusions

In this paper we present the results obtained by a new global mascon processing method, whereby we focus on the mass balances of the Antarctic Ice Sheet (AIS), the Greenland Ice Sheet (GrIS), and the Land glaciers and Ice Caps (LIC) signal in an attempt to assess the mass flux contributing to the global sea level. A sensitivity analysis of the mascon algorithm shows that the largest uncertainty in the predicted mass-time series come from updating the GIA model for the AIS. Other significant effects concern the selection of the time window and the consequences replacing the degree 2 gravitational flattening parameter and adding the degree 1 loading terms that are poorly or not observed by GRACE. A summary of our findings is the following:

1. Since 2010, GRACE shows a remarkable speed up of the global mass loss. We find −480 ± 36 Gt/yr between 2003 and 2010 for the combined signal of the GrIS, the AIS, and the LIC. For comparison, we get −532 ± 34 Gy/yr for the mass loss between February 2003 and June 2013. For this, we corrected the LIC signal with a GLDAS model prediction and applied the alternative GIA model ensemble for the GrIS and the AIS. The hypothesis that we observed different rates of mass loss tests positive within 95% probability.
2. The uncertainty of the mass balance estimates is not only determined by data variability and the length of the time window but also by GIA modeling uncertainties. GRACE solutions based upon an ensemble of updated GIA models with new ice history models as discussed in section 2.1.1 show for Greenland −278 ± 19 Gt/yr between February 2003 and June 2013 which is statistically seen indistinguishable from mass loss rates obtained with the ICE-5G VM2 solution.
3. The mass balance for the Antarctic is significantly affected by selection of two new GIA models. We used the IJ05_R2 GIA model and allowed for different choices in the viscosity space in the upper and lower mantles and the lithospheric thickness and found a mass balance of −93 ± 29 Gt/yr. Similar analyses with the W12a model are obtained −91 ± 23 Gt/yr between February 2003 and June 2013.
4. The consequence of not applying the geocenter loading corrections or replacing the gravitational flattening terms mostly affects the mass balance of the AIS. With a method that is independent from *Swenson et al.* [2008] we arrive at a rate of change of −0.21 mm/yr for the *z* axis of the geocenter which reduces the Antarctic mass balance by 33 Gt/yr. By replacing the gravitational flattening parameter with a value from satellite laser ranging, we find that the AIS mass balance decreases by 46 Gt/yr.
5. Our estimates for the LIC signal are close to the values found by *Jacob et al.* [2012] and both GRACE methods discussed in *Gardner et al.* [2013] who remark that classical glaciologic estimates for the mass balances of glaciers outside the Greenland and Antarctic ice sheets are more negative than those obtained with satellite gravimetry. The paper of *Gardner et al.* [2013] accounts −38 ± 7 Gt/yr to peripherical glaciers of Greenland and −6 ± 10 Gt/yr to the Antarctica and the sub-Antarctic which are already contained in our estimates. The remaining signal without Greenland and the Antarctic in *Gardner et al.* [2013] is however larger than what we recovered in the LIC signal. Differences between the GRACE only results for the LIC discussed in *Gardner et al.* [2013] can be explained by the fact that hydrology corrections are handled differently. Nevertheless, both GRACE approaches do not lead to statistically significant differences in the rate of mass loss of the total LIC signal.

From our results, it can be concluded that the total contribution to a sea level rise signal becomes 1.66 ± 0.07 mm/yr (603 ± 26 Gt/yr) between February 2003 and June 2013 when only the ICE-5G GIA model is used. Input to this analysis is the combination of the mass-time series of the GrIS, the AIS, and the LIC. In *Ivins et al.* [2013] a change in sea level was reported by use of a new Antarctic IJ05_R2 GIA model, when the

AIS mass balance is derived as an ensemble estimate involving the GIA models from IJ05_R2 and W12a for the AIS the contribution to the sea level becomes 1.47 ± 0.09 mm/yr or 532 ± 34 Gt/yr.

Continental water storage on regions outside the AIS, the GrIS, and LIC GRACE show continental water storage changes that are latitude dependent. Between February 2003 and June 2013, GRACE shows a mass gain at tropical latitudes while the continents become dryer at subtropical and moderate latitudes with rates up to 7 mm/yr. We did not find an integrated effect in this domain that is statistically significant different from zero.

We take note that several domains in Table 5 display statistically significant accelerations in mass change that do not depend on GIA modeling. Noticeable is for instance an acceleration of mass loss on West Antarctica and in particular within the Amundsen sector. Accelerations are also persistent on the Greenland Ice Sheet and the corresponding melt water flux into the oceans. The 95% confidence level of the acceleration terms is in our opinion statistically significant between February 2003 and June 2013, under the assumption that the GRACE time series observations are not correlated.

A sea level rise signal of 532 ± 34 Gt/yr comes with an acceleration of 42 ± 33Gt/yr^2 so that we project 26 ± 16 cm of sea level change in 2050 and 112 ± 77 cm in 2100 under the assumption that the present-day acceleration is sustained. Given the relative short time series of GRACE the observed accelerations may also be the result of interannual variability. Whether an acceleration from glacier mass flux can be maintained for such a long period is therefore a topic for research; see also *Wouters et al.* [2013a]. Accelerations of the total sea level from tide gauges have been reported by *Woodworth et al.* [2011] who shows values smaller than 0.01 mm/yr^2 on century time scales. The sea level acceleration found by GRACE is significantly different compared to the present day of sea level rise of 3.2 ± 0.4 mm/yr from satellite altimetry and 2.8 ± 0.8 mm/yr from a combination of tide gauges and satellite altimetry (time window: 1993–2009); for a discussion, see *Church et al.* [2011] and *Church and White* [2011].

Whether the sea level budget is closed depends on the quality and coverage of the sea level rise signal following from density; see also *Leuliette and Willis* [2011] where it is explained that density measurements are well covered up to 2000 m depth with ARGO profiling float data and other XBT and CTD data. Our estimate for the total density-driven part of the sea level rise signal not observed by GRACE is the difference between the value of satellite altimetry and GRACE-derived mass balances, for which we get with the newer GIA models for the AIS: 1.7 ± 0.4 mm/yr when altimetry is used to measure the total sea level signal or 1.3 ± 0.8 mm/yr when a combination of tide gauges and altimetry is used. As a result approximately half of the present-day sea level rise consists of mass change, while the remaining part is density driven.

Appendix A: Mascon Generation Algorithm

The centroid and radius of each mascon follow from a triangulation algorithm that starts with an icosahedron projected on a unit sphere. Successive subdivisions of the icosahedron cause each triangular face to be divided into four new triangles by recursion step. The algorithm bisects the sides of a triangle at recursion step i and connects the bisection points and the corners at level i to generate four nonoverlapping triangles at recursion step $i + 1$. This procedure is repeated until a certain threshold level (in our case 6) is reached. After the final recursion step, each vertex of the triangulated surface (where the triangles meet) defines the centroid of a dish where the mascon radius is chosen such that it spans one third of the total area of all triangles joining at the vertex.

This algorithm yields a set of nearly equal area mascons that are homogeneously distributed over the Earth's surface, the integral of all mascon areas is $4\pi \times a_e^2$. At level 5 the algorithm returns 2562 mascons with an average spherical radius of 2.26°; the smallest and largest mascons have a radius of 1.99° and 2.47°. At level 6 we find a total of 10,242 mascons where the dishes have a minimum radius of 1.00°, a mean value of 1.13°, and a maximum at 1.24°. The level 6 set of 10,242 mascons is considered to be a reference for estimating ice sheet and glacier mass balances while our contribution to the IMBIE study of *Shepherd et al.* [2012] was based on 2562 mascons. For the level 6 mascon set, we oversample the geopotential field, since it originally consists of 3717 coefficients originating from a $L = 60$ spherical harmonic expansion. For the main ice caps, the refinement of the mascons at level 6 did not significantly affect our mass balances estimations.

Appendix B: Effect of Spatial Averaging on Mascon Inversion Results

An alternative way to formulate the basin influence functions is

$$\beta_k(\psi_k, \tau_\mathrm{P}, L, R) = \sum_{l=0}^{L} W_l^\mathrm{P}(\tau_\mathrm{P})\gamma_l(R)\bar{P}_l(\cos\psi_k) \tag{B1}$$

where an additional isotropic mascon influence in the form of a spatial averaging function $W_l^\mathrm{P}(\tau_\mathrm{P})$ is considered during the convolution. The averaging function is

$$W_l^\mathrm{P}(\tau_\mathrm{P}) = \cot\left(\frac{\psi_0}{2}\right)\frac{P_{l1}(\cos\psi_0)}{l(l+1)} \tag{B2}$$

with $\psi_0 = \tau_\mathrm{P}(\pi)^{-1/2}$ so that the area of the dish mentioned in *Rapp* [1977] approximates the side length τ_P of the spherical block in the Pellinen tapering function. The purpose of $W_l^\mathrm{P}(\tau_\mathrm{P})$ is to be able to study the effect of spatial smoothing on the rate of mass change obtained with the mascon inversion method. We varied the parameter τ_P between 0° and 4°; for 0°, we get $W_l^\mathrm{P}(0) = 1$, where for all studied areas the lowest mass changes are found with the mascon method. For $\tau_\mathrm{P} = 2°$, all computed mass changes scale by 1% (meaning that the rate of mass change increases in either direction by 1%), and for 4°, the scale factor is $\approx$ 4.7%. Our conclusion is therefore that the mascon algorithm is mostly insensitive to additional averaging functions $W_l^\mathrm{P}(\tau_\mathrm{P})$ in the mascon influence function and that spatial averaging results in scaled versions of the computed time series.

Acknowledgments
The authors thank the European Space Agency and the National Aeronautics and Space Administration for their financial support to the ice sheet mass balances intercomparison experiment IMBIE in 2011 and 2012.

References

A, G., J. Wahr, and S. Zhong (2013), Computations of the viscoelastic response of a 3-D compressible Earth to surface loading: An application to glacial isostatic adjustment in Antarctica and Canada, *Geophys. J. Int.*, *192*, 557–572, doi:10.1093/gji/ggs030.

Anderson, E., Z. Bai, J. Dongarra, A. Greenbaum, A. McKenney, J. Du Croz, S. Hammerling, J. Demmel, C. Bischof, and D. Sorensen (1990), LAPACK: A portable linear algebra library for high-performance computers, in *Proceedings of the 1990 ACM/IEEE Conference on Supercomputing, Supercomputing '90*, IEEE Computer Society Press, Los Alamitos, Calif. [Available at http://dl.acm.org/citation.cfm?id=110382.110385.]

Baur, O., and N. Sneeuw (2011), Assessing Greenland ice mass loss by means of point-mass modelling: A viable methodology, *J. Geod.*, *85*, 607–615, doi:10.1007/s00190-011-0463-1.

Blewitt, G., D. E. Lavallée, P. Clarke, and K. Nurutdinov (2001), A new global mode of Earth deformation: Seasonal cycle detected, *Science*, *294*, 2342–2345, doi:10.1126/science.1065328.

Blewitt, G. (2003), Self-consistency in reference frames, geocenter definition, and surface loading of the solid Earth, *J. Geophys. Res.*, *108*(B2), 2103, doi:10.1029/2002JB002082.

Bettadpur, S. (2007), GRACE 32-742, UTCSR level-2 processing standards document for level-2 product release 004, 27-Feb-2007. [Available at ftp://podaac.jpl.nasa.gov/allDate/grace/docs.]

Boening, C., M. Lebsock, F. Landerer, and G. Stephens (2012), Snowfall-driven mass change on the East Antarctic ice sheet, *Geophys. Res. Lett.*, *39*, L21501, doi:10.1029/2012GL053316.

Cheng, M., B. D. Tapley, and J. C. Ries (2013), Deceleration in the Earth's oblateness, *J. Geophys. Res. Solid Earth*, *118*, 740–747, doi:10.1002/jgrb.50058.

Church, J. A., and N. J. White (2011), Sea-level rise from the late 19th to the early 21st century, *Surv. Geophys.*, *32*, 585–602, doi:10.1007/s10712-011-9119-1.

Church, J. A., N. J. White, L. F. Konikow, C. M. Domingue, J. G. Cogley, E. Rignot, J. M. Gregory, M. R. van den Broeke, A. J. Monaghan, and I. Velicogna (2011), Revisiting the Earth's sea-level and energy budgets from 1961 to 2008, *Geophys. Res. Lett.*, *38*, L18601, doi:10.1029/2011GL048794.

Dahlen, F. A. (1976), The passive influence of the oceans upon the rotation of the Earth, *Geophys. J. R. Astron. Soc.*, *46*, 363–406.

Dobslaw, H., F. Flechtner, I. Bergmann-Wolf, C. Dahle, R. Dill, S. Esselborn, I. Sasgen, and M. Thomas (2013), Simulating high-frequency atmosphere-ocean mass variability for dealiasing of satellite gravity observations: AOD1B RL05, *J. Geophys. Res. Oceans*, *118*, 3704–3711, doi:10.1002/jgrc.20271.

Eicker, A., J. Schall, and J. Kusche (2014), Regional gravity modelling from spaceborne data: Case studies with GOCE, *Geophys. J. Int.*, *196*, 1431–1440, doi:10.1093/gji/ggt485.

Evelpidou, N., P. Pirazzoli, A. Vassilopoulos, G. Spada, G. Ruggieri, and A. Tomasin (2012), Late Holocene sea level reconstruction based on observations of Roman fish tanks, Tyrrhenian Coast of Italy, *Geoarchaeology*, *27*, 259–277.

Farrell, W. E. (1972), Deformation of the Earth by surface loads, *Rev. Geophys.*, *10*(3), 761–797, doi:10.1029/RG010i003p00761.

Fleming, K., and K. Lambeck (2004), Constraints on the Greenland Ice Sheet since the Last Glacial Maximum from sea-level observations and glacial-rebound models, *Quat. Sci. Rev.*, *23*, 1053–1077.

Gardner, A. S., et al. (2013), A reconciled estimate of glacier contributions to sea level rise: 2003 to 2009, *Science*, *340*, 852–857, doi:10.1126/science.1234532.

Global Land Ice Measurements From Space (GLIMS), and National Snow and Ice Data Center (NSIDC) (2013), *Global Land Ice Measurements From Space Glacier Database*, Compiled and made available by the international GLIMS community and the National Snow and Ice Data Center, Boulder, Colo., doi:10.7265/N5V98602.

Gunter, B., T. Urban, R. Riva, M. Helsen, R. Harpold, S. Poole, P. Nagel, B. Schutz, and B. Tapley (2009), A comparison of coincident GRACE and ICESat data over Antarctica, *J. Geod.*, *83*, 1051–1060.

Han, D., and J. M. Wahr (1995), The viscoelastic relaxation of a realistically stratified Earth, and a further analysis of postglacial rebound, *Geophys. J. Int.*, *120*, 287–311.

Intergovernmental Panel on Climate Change (2013), Climate change 2013—The physical science basis, in *Working Group I Contribution to the Fifth Assessment Report of the Intergovernmental Panel on Climate Change*, edited by D. Qin, S. K. Allen, and M. M. B. Tignor, 1535 pp., Cambridge Univ. Press, Cambridge, U. K., ISBN 9781107661820.

Ivins, E. R., M. M. Watkins, D. N. Yuan, R. Dietrich, G. G Casassa, and A. Rülke (2011), On-land ice loss and glacial isostatic adjustment at the Drake Passage: 2003–2009, *J. Geophys. Res.*, *116*, B02403, doi:10.1029/2010JB007607.

Ivins, E. R., T. S. James, J. Wahr, E. Schrama, F. Landerer, and K. Simon (2013), Antarctic contribution to sea-level rise observed by GRACE with improved GIA correction, *J. Geophys. Res. Solid Earth*, *118*, 3126–3141, doi:10.1002/jgrb.50208.

Jacob, T., J. Wahr, W. T. Pfeffer, and S. Swenson (2012), Recent contributions of glaciers and ice caps to sea level rise, *Nature*, *482*, 514–518.

James, T. S., and E. R. Ivins (1995), Present-day Antarctic ice mass changes and crustal motion, *Geophys. Res. Lett.*, *22*(8), 973–976, doi:10.1029/94GL02800.

Jensen, L., R. Rietbroek, and J. Kusche (2013), Land water contribution to sea level from GRACE and Jason-1 measurements, *J. Geophys. Res. Oceans*, *118*, 212–226, doi:10.1002/jgrc.20058.

Killett, B., J. Wahr, S. Desai, D. Yuan, and M. Watkins (2011), Arctic Ocean tides from GRACE satellite accelerations, *J. Geophys. Res.*, *116*, C11005, doi:10.1029/2011JC007111.

Koch, K. R. (1999), *Parameter Estimation and Hypothesis Testing in Linear Models*, Springer Verlag, New York, ISBN 978-3-540-65257-1.

Lavallée, D. A., T. van Dam, G. Blewitt, and P. J. Clarke (2006), Geocenter motions from GPS: A unified observation model, *J. Geophys. Res.*, *111*, B05405, doi:10.1029/2005JB003784.

Leuliette, E. W., and J. K. Willis (2011), Balancing the sea level budget, *Oceanography*, *24*(2), 122–129, doi:10.5670/oceanog.2011.32.

Luthcke, S. B., T. J. Sabaka, B. D. Loomis, A. A. Arendt, J. J. McCarthy, and J. Camp (2013), Antarctica, Greenland and Gulf of Alaska land-ice evolution from an iterated GRACE global mascon solution, *J. Glaciol.*, *59*(216), 613–631, doi:10.3189/2013JoG12J147.

Muller, P. M., and W. L. Sjogren (1968), Mascons: Lunar mass concentrations, *Science*, *161*, 680–684.

Paul, M K (1978), Recurrence relations for integrals of associated Legendre functions, *B. Géod.*, *52*(3), 177–190.

Paulson, A., S. Zhong, and J. Wahr (2007), Inference of mantle viscosity from GRACE and relative sea level data, *Geophys. J. Int.*, *171*, 497–508, doi:10.1111/j.1365-246X.2007.03556.x.

Peltier, W. R. (2004), Global glacial isostasy and the surface of the Ice-Age Earth: The ICE-5G (VM2) model and GRACE, *Annu. Rev. Earth Planet. Sci.*, *32*, 111–149.

Press, W. H., B. P. Flannery, S. A. Teukolsky, and W. T. Vetterling (1989), *Numerical Recipes, The Art of Scientific Computing*, Cambridge Univ. Press, New York, ISBN 0521383307.

Rapp, R. H. (1977), The relationship between mean anomaly block sizes and spherical harmonic representations, *J. Geophys. Res.*, *82*(33), 5360–5364.

Raup, B. H., A. Racoviteanu, S. J. S. Khalsa, C. Helm, R. Armstrong, and Y. Arnaud (2007), The GLIMS Geospatial glacier database: A new tool for studying glacier change, *Global Planet. Change*, *56*, 101–110, doi:10.1016/j.gloplacha.2006.07.018.

Rietbroek, R., S. E. Brunnabend, J. Kusche, and J. Schröter (2012a), Resolving sea level contributions by identifying fingerprints in time-variable gravity and altimetry, *J. Geodyn.*, *59–60*, 72–81, doi:10.1016/j.jog.2011.06.007.

Rietbroek, R., M. Fritsche, S. E. Brunnabend, I. Daras, J. Kusche, J. Schroeter, F. Flechtner, and R. Dietrich (2012b), Global surface mass from a new combination of GRACE, modeling OBP and reprocessed GPS data, *J. Geodyn.*, *59–60*, 64–71, doi:10.1016/j.jog.2011.02.003.

Riva, R. E. M., J. L. Bamber, D. A. Lavallée, and B. Wouters (2010), Sea-level fingerprint of continental water and ice mass change from GRACE, *Geophys. Res. Lett.*, *37*, L19605, doi:10.1029/2010GL044770.

Rodell, M., et al. (2004), The global land data assimilation system, *Bull. Am. Meteorol. Soc.*, *85*(3), 381–394.

Sabadini, R., and L. L. A. Vermeersen (2004), *Global Dynamics of the Earth, Applications of Normal Mode Relaxation Theory to Solid-Earth Geophysics*, Kluwer Acad., Dordrecht, Netherlands, ISBN 1-4020-1267-5.

Schrama, E. J. O., and B. Wouters (2011), Revisiting Greenland ice sheet mass loss observed by GRACE, *J. Geophys. Res.*, *116*, B02407, doi:10.1029/2009JB006847.

Schrama, E. J. O., B. Wouters, and D. E. Lavallée (2007), Signal and noise in Gravity Recovery And Climate Experiment (GRACE) observed surface mass variations, *J. Geophys. Res.*, *B8*, B08407, doi:10.1029/2006JB004882.

Schrama, E. J. O., B. Wouters, and L. L. A. Vermeersen (2011), Present day regional mass loss of Greenland observed with satellite gravimetry, *Surv. Geophys.*, *32*, 377–385, doi:10.1007/s10712-011-9113-7.

Shepherd, A., et al. (2012), A reconciled estimate of ice sheet mass balance, *Science*, *338*(6111), 1183–1189, doi:10.1126/science.1228102.

Simpson, M. J. R., G. A. Milne, P. Huybrechts, and A. J. Long (2009), Calibrating a glaciological model of the Greenland ice sheet from the Last Glacial Maximum to present-day using field observations of relative sea level and ice extent, *Quat. Sci. Rev.*, *28*, 1631–1657, doi:10.1016/j.quascirev.2009.03.004.

Spada, G., V. R. Barletta, V. Klemann, R. E. M. Riva, Z. Martinec, P. Gasperini, B. Lund, D. Wolf, L. L. A. Vermeersen, and M. A. King (2011), A benchmark study for glacial isostatic adjustment codes, *Geophys. J. Int.*, *185*, 106–132, doi:10.1111/j.1365-246X.2011.04952.x.

Swenson, S., and J. Wahr (2002), Methods for inferring regional surface-mass anomalies from Gravity Recovery and Climate Experiment (GRACE) measurements of time-variable gravity, *J. Geophys. Res.*, *107*(B09), 2193, doi:10.1029/2001JB000576.

Swenson, S., D. Chambers, and J. Wahr (2008), Estimating geocenter variations from a combination of GRACE and ocean model output, *J. Geophys. Res.*, *113*, B08410, doi:10.1029/2007JB005338.

Tapley, B. D., S. Bettadpur, J. C. Ries, P. F. Thompson, and M. M. Watkins (2004), GRACE measurements of mass variability in the Earth system, *Science*, *305*, 503–505.

van den Broeke, M., J. Bamber, J. Ettema, E. Rignot, E. Schrama, J. W. van den Berg, E. van Meijgaard, I. Velicogna, and B. Wouters (2009), Partitioning recent Greenland mass loss, *Science*, *326*(5955), 984–986, doi:10.1126/science.1178176.

Velicogna, I. (2009), Increased rates of mass loss from the Greenland and Antarctic ice sheets revealed by GRACE, *Geophys. Res. Lett.*, *36*, L19503, doi:10.1029/2009GL040222.

Wahr, J., M. Molenaar, and F. Bryan (1998), Time variability of the Earth's gravity field: Hydrological and oceanic effects and their possible detection using GRACE, *J. Geophys. Res.*, *103*(B12), 30,205–30,229.

Wahr, J., D. Wingham, and C. Bentley (2000), A method of combining ICESat and GRACE satellite data to constrain Antarctic mass balance, *J. Geophys. Res.*, *105*(B7), 16,279–16,294, doi:10.1029/2000JB900113.

Whitehouse, P. L., M. J. Bentley, and A. M. Le Brocq (2012a), A deglacial model for Antarctica: Geological constraints and glaciological modeling as a basis for a new model of Antarctic glacial isostatic adjustment, *Quat. Sci. Rev.*, *32*, 1–24.

Whitehouse, P. L., M. J. Bentley, G. A. Milne, M. A. King, and I. D. Thomas (2012b), A new glacial isostatic adjustment model for Antarctica: Calibrated and tested using observations of relative sea-level change and present-day uplift rates, *Geophys. J. Int.*, *190*, 1464–1482.

Woodworth, P. L., M. Meneédez, and W. R. Gehrels (2011), Evidence for century-timescale acceleration in mean sea levels and for recent changes in extreme sea level, *Surv. Geophys.*, *32*, 619, doi:10.1007/s10712-011-9112-8.

Wouters, B. (2010), Identification and modeling of sea level change contributors: On GRACE satellite gravity data and their applications to climate monitoring, PhD thesis, Delft University of Technology, Delft, Netherlands, ISBN 9789061323167.

Wouters, B., D. Chambers, and E. J. O. Schrama (2008), GRACE observes small-scale mass loss in Greenland, *Geophys. Res. Lett.*, *35*, L20501, doi:10.1029/2008GL034816.

Wouters, B., J. L. Bamber, M. R. van den Broeke, J. T. M. Lenaerts, and I. Sasgen (2013a), Limits in detecting acceleration of ice sheet mass loss due to climate variability, *Nat. Geosci.*, *6*, 613–616, doi:10.1038/ngeo1874.

Wouters, B., J. Wahr, A. Gardner, and G. Moholdt (2013b), How well does GRACE capture small-scale glacier mass variations, Abstract presented at 2013 EGU General Assembly, Vienna, Austria, 7–12 April.

Zwally, H. J., M. B. Giovinetto, M. A. Beckley, and J. L. Saba (2012), Goddard Space Flight Center Cryospheric Sciences Laboratory, Greenbelt, Md. [Available at http://icesat4.gsfc.nasa.gov/cryo_data/ant_grn_drainage_systems.php.]